Frequency modulated atomic force microscopy on MgO(001) thin films: interpretation of atomic image resolution and distance dependence of tip–sample interaction

2006 Nanotechnology 17 S101

(http://iopscience.iop.org/0957-4484/17/7/S01)

INSTITUTE OF PHYSICS PUBLISHING NANOTECHNOLOGY
Nanotechnology **17** (2006) S101–S106 doi:10.1088/0957-4484/17/7/S01

Frequency modulated atomic force microscopy on MgO(001) thin films: interpretation of atomic image resolution and distance dependence of tip–sample interaction

M Heyde, M Sterrer, H-P Rust and H-J Freund

Fritz-Haber-Institut der Max-Planck-Gesellschaft, Faradayweg 4-6, D-14195 Berlin, Germany

E-mail: heyde@fhi-berlin.mpg.de

Received 22 August 2005, in final form 6 December 2005
Published 10 March 2006
Online at stacks.iop.org/Nano/17/S101

Abstract
Atomically resolved images on a MgO(001) thin film deposited on Ag(001) obtained in ultrahigh vacuum by frequency modulated atomic force microscopy at low temperature are presented and analysed. Images obtained in the attractive regime show a different type of contrast formation from those acquired in the repulsive regime. For the interpretation of the image contrast we have investigated the tip–sample interaction. Force and energy were recovered from frequency shift versus distance curves. The derived force curves have been compared to the force laws of long-range, short-range and contact forces. In the attractive regime close to the minimum of the force–distance curve elastic deformations have been confirmed. The recovered energy curve has been scaled to the universal Rydberg model, yielding a decay length of $l = 0.3$ nm and $\Delta E = 4.2$ aJ (26 eV) for the maximum adhesion energy. A universal binding-energy–distance relation is confirmed for the MgO(001) thin film.

1. Introduction

Frequency modulated atomic force microscopy (FM-AFM) has shown its ability to image surfaces of different materials at the atomic level [1–4]. However, proper descriptions of the tip–sample interaction and contrast mechanisms are still under discussion. In scanning tunnelling microscopy, the model of Tersoff and Hamann [5] provides a simple picture of operation based on topography and local density of states at the surface. Yet, for the AFM such a simple model does not exist. The level of complexity needed to calculate the tip–sample interaction in FM-AFM depends on the properties of the system being studied [6, 7]. For the interaction of ionic systems atomistic simulation methods based on a classical interatomic potential treatment and the shell model for ionic polarization allow for a qualitative description. Although even quantitative agreement with experiments has been achieved in some cases, these models remain highly idealized. Quantitative modelling of specific images relies on parameters which cannot be determined easily in experiment. For example, the tip radius and its actual separation from the surface are not directly known. Also the chemical nature of the tip significantly affects the images and it may even reverse contrast [8]. For a quantitative understanding of FM-AFM and its applications there is thus considerable interest in experiments which cast light on these phenomena. In this study, we present atomically resolved FM-AFM images and force–distance curves obtained from the surface of a thin MgO film and address different imaging contrast mechanisms.

2. Experimental setup

The experiments were performed in a custom-made Eigler-style ultrahigh vacuum low-temperature microscope [9], which is equipped with a double quartz tuning fork sensor. The

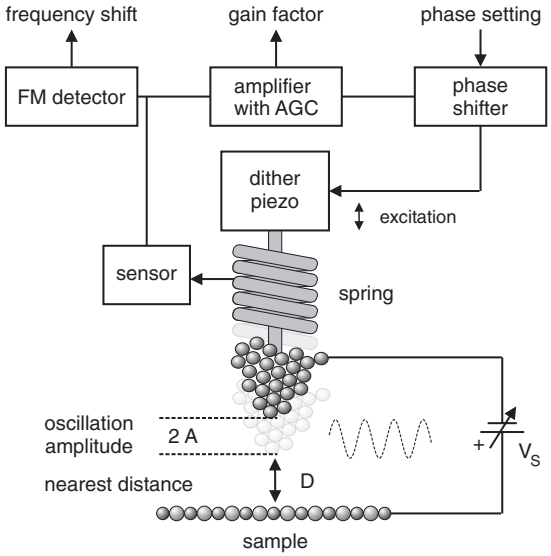

Figure 1. Schematic setup of FM-AFM operated in UHV and a definition of the parameters A and D.

microscope allows operation in STM and AFM mode. The sensor has a resonance frequency of $f_0 = 17\,444$ Hz, a Q-factor of $Q = 12\,500$ and a stiffness of $k = 30\,000$ N m^{-1}. The spring constant has been calibrated by observing the frequency shift in the resonant frequency when adding a known mass to the force sensor [10]. Such an experiment has been performed by adding a metallic sphere to a double tuning fork test assembly. The obtained results are also in good agreement with finite element calculations [11]. Our double quartz tuning fork setup works at small oscillation amplitudes in the range of $A = 0.4$ nm. A cut Pt/Ir wire with a diameter of 0.25 mm has been used as a tip. A schematic setup of FM-AFM operated in a self-exciting oscillation mode is provided in figure 1. The detected oscillation amplitude signal is fed into an automatic gain control (AGC) circuit and is used to excite the spring system mechanically by a dither-piezo. A phase shifter ensures that the spring system is excited at its resonance frequency [12]. Further details of the experimental setup have been described elsewhere [13, 14].

The Ag(001) substrate was cleaned by repeated Ar^+ sputtering (800 V, 10 μA cm^{-2}) and subsequent annealing to 700 K. MgO films were grown by reactive deposition of Mg in an oxygen pressure of 1×10^{-6} mbar at a substrate temperature of 550 K. The MgO deposition rate was 0.75 ML min^{-1}. The AFM measurements were carried out at 5 K.

3. Results and discussion

Figure 2(a) shows a high-resolution image controlled to a constant frequency shift in the attractive mode ($\Delta f = -3.7$ Hz) of the surface of 4 ML MgO(001)/Ag(001). The grey scale gives the z-displacement. It is a general finding in FM-AFM imaging of ionic surfaces that only one type of ion is imaged [15–17]. The FM-AFM imaging process in the attractive regime of ionic tip–surface systems has been well described in the literature [18]. The two dashed rectangles in figure 2(a) mark the position of the two different ionic species.

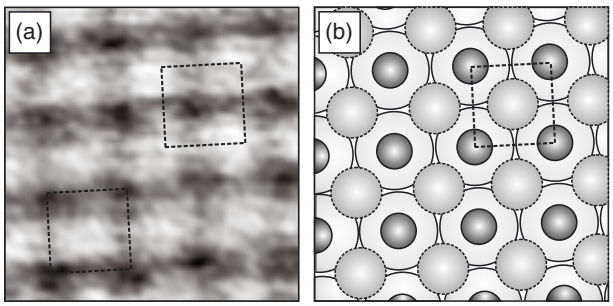

Figure 2. (a) FM-AFM image of MgO on Ag(001) with atomic resolution obtained in the attractive regime. Scan area 1.1 nm by 1.1 nm, $\Delta f = -3.8$ Hz, $A = 0.35$ nm, $T = 5$ K, approximately 11 pm corrugation. (b) Schematic illustration of the MgO/Ag(001) growth model: Mg-atoms occupy hollow sites, i.e. they continue the Ag fcc lattice in the z-direction ($a = 0.409$ nm); O-atoms prefer on-top sites. The unit cells of different ionic species are marked in both images by dashed rectangles.

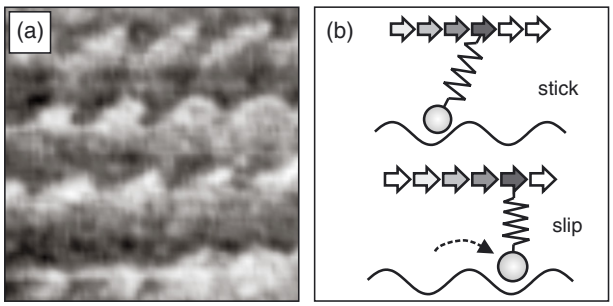

Figure 3. (a) FM-AFM image of MgO on Ag(001) with atomic resolution recorded in the repulsive regime. Scan area 1.1 nm by 1.1 nm, $\Delta f = +3.8$ Hz, $A = 0.35$ nm, $T = 5$ K, approximately 18 pm corrugation. (b) Schematic model of the stick–slip-process. The time evolution during the scan along the x-direction is illustrated.

While one type of ion is imaged as a protrusion (bright), the other one is given by a depression (dark). Figure 2(b) provides a schematically illustrated growth model of MgO on Ag(001). The assignment of the dashed rectangles is randomly picked. From the presented measurements we cannot directly determine if the protrusions correspond to O- or Mg-sites. To gain some more insights into the imaging contrast, we varied the frequency shift set-point. The switching between the attractive and the repulsive mode has been performed by adjusting the set-point of our feedback electronics [14]. In figure 3(a) an image of MgO obtained in the repulsive mode ($\Delta f = +3.7$ Hz) is given. The switching between the attractive and the repulsive regime imaging has been repeated several times and the obtained data reveal a similar conversion in the imaging contrast. The mechanism of contrast formation of ionic surfaces is known for FM-AFM imaging in the attractive mode [15]. However, for FM-AFM images contrast formation in the repulsive mode has only been studied for CaF_2 and MgO so far [19, 14]. The features of the observed imaging contrast in the repulsive regime behave like a typical stick–slip movement [20]. These have been analysed in figure 3(a), where the contours of the imaging contrast show a triangular shape. The simple Tomlinson model [21] can be used to simulate the

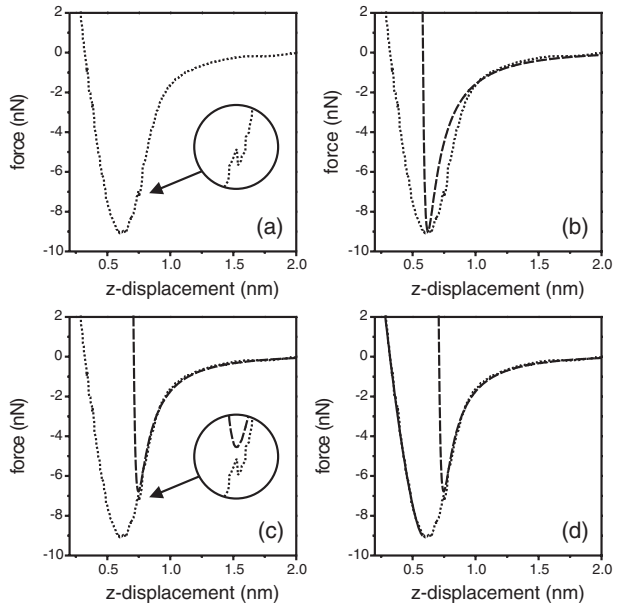

Figure 4. (a) The dotted line represents the recovered force of the measured frequency shift over z-displacement obtained by equation (1). The arrow marks the point where a kink is visible in the force–distance curve combined with a magnification of this region. (b) The dashed line represents a fit of equation (2) to the minimum of the force–distance curve. (c) The best fit using equation (2) for the attractive regime. (d) The same as (c) with an additional curve where the best fit for the repulsive regime obtained by equation (3) is given by a solid line.

movement of an AFM tip on the sample surface. It reveals indeed that the AFM tip moves in a stick–slip type movement over the sample surface [22, 23]. In such a case the image contrast is dominated by the preferred paths of the tip over the sample surface. A schematic illustration of this tip movement is given in figure 3(b) for the x-direction.

For a more detailed interpretation of tip–sample interactions, distance-dependent frequency shift measurements have been performed. To calculate the interaction force $F(D)$ between the tip and the sample, formula (1) has been used [24]. This formula allows the determination of $F(D)$ from the frequency shift, and is valid for any oscillation amplitude. The expression for the force in terms of the frequency shift is given by

$$F(D) = \frac{2k}{f_0}\int_D^\infty \Delta f(z)\left(\left(1+\frac{A^{1/2}}{8\sqrt{\pi(z-D)}}\right) - \frac{A^{3/2}}{\sqrt{2(z-D)}}\frac{\mathrm{d}}{\mathrm{d}z}\right)\mathrm{d}z \qquad (1)$$

where D is the distance of closest approach between the tip and the sample, z is the tip–sample distance, and F is the interaction force between the tip and the sample. The derived force–distance curve is plotted by a dotted line in each of the four graphs (a)–(d) of figure 4. A small kink in the curve close before the minimum has been magnified in graphs (a) and (c).

For the identification of different force contributions we started to fit the experimental force curve with different types of force laws. A suitable description of the force between the tip and the sample is provided by a combination of a long-range (van der Waals) and a short-range (Lennard-Jones) term. This results in the sample force

$$F_{\mathrm{ts}}(z) = -\frac{A_{\mathrm{H}}R}{6z^2} + \frac{12E_0}{r_0}\left[\left(\frac{r_0}{z}\right)^{13} - \left(\frac{r_0}{z}\right)^{7}\right], \qquad (2)$$

where A_{H} is the Hamaker constant, R the tip radius, E_0 the binding energy, and r_0 the equilibrium distance of the Lennard-Jones potential [25]. This model is valid as long as the tip and the sample are not in contact and elastic contact forces can be neglected. In figure 4(b) a comparison of the force–distance curve with the force law of equation (2) (dashed line) is given, where the parameters have been set to fit to the minimum of the force–distance curve. Both the repulsive and attractive parts of the recovered force–distance curve cannot be correlated by the curve shape calculated from equation (2). In figure 4(c) a fit to the attractive part of the force–distance curve has been performed. The attractive regime of the force–distance curve is very well matched, but only before the minimum is reached. The deep and wide minimum of the recovered force curve cannot be described accurately by equation (2). The experimental data of the recovered force curve cannot be fully fitted by the Lennard-Jones force, which has a steep increase in the repulsive regime. Selecting another short-range interaction potential like the Morse [26] or the Stillinger–Weber potential [27] does not lead to a better agreement. It is obvious that elastic deformations contribute to the tip–sample interaction even close before the minimum of the force–distance curve is reached. The kink marked in the inset of figure 4(a) seems to indicate a transition point at which the elastic deformations contribute significantly to the tip–sample interaction. However, we have to admit that not all obtained curves provide a kink at the same position. Nevertheless, for a stable tip–sample configuration the shape of the curves is reproducible. If the tip comes closer to the sample surface, the attractive force between the tip and the sample dominates. The marked point seems to indicate a critical tip–surface distance at which surface ions strongly displace from their equilibrium position, causing a change in the tip–surface interaction. Calculations for an ionic nanotip interacting with an ionic surface predict strong displacements of surface ions in the tip and the sample at small tip–surface distances [28]. The atomic resolution in the attractive regime has been obtained at a set-point around the position where the kink in the force–distance curve appears. Also in STM imaging elastic deformation of the tip apex mediated by adhesive tip–sample interactions is made responsible for the resolution of atomic corrugation [29, 30]. Similar effects have been reported by Sugawara *et al* for atomic resolution FM-AFM imaging of the InP(110) surface [31].

For the interpretation of the purely repulsive regime we have used the Hertz theory [32], where elastic tip–sample forces are considered. Such a model has been successfully used to describe the tip–sample contact of an AFM [33, 34]. It results in a contact force law of the type

$$F_{\mathrm{c}}(z) = g_0(z_0 - z)^{3/2} + F_{\mathrm{ad}} \qquad (3)$$

for $z \leqslant z_0$ [35]. F_{ad} is the maximum adhesion force between the tip and the sample surface, z_0 is the distance of separation at point F_{ad}, and g_0 is a constant that depends on

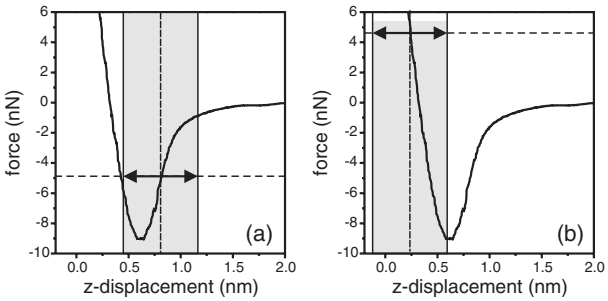

Figure 5. In graph (a) the grey shaded area marks schematically the z-range at which the tip is oscillating over the sample surface with $A = 0.4$ nm when imaging in the attractive regime. In graph (b), the same area is marked for a set-point in the repulsive regime.

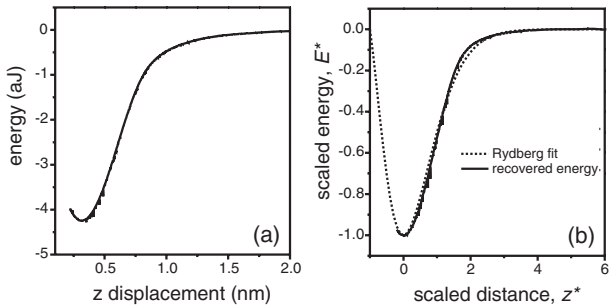

Figure 6. (a) The solid line represents the recovered energy of the measured frequency shift over z-displacement obtained by equation (4). (b) The scaled recovered energy over separation of (a) together with the full plotted curve of the Rydberg function (dotted line) given by equation (7). The scaling parameters were $\Delta E = 4.2$ aJ (26 eV) for maximum adhesion and $l = 0.3$ nm for the decay length.

the elasticity of the tip and the sample and on the shape of the tip. A fit of equation (3) to the recovered force–distance curve is shown in figure 4(d) by a solid line. The good agreement with the experimental force curve demonstrates that the elastic contact force given by the Hertz theory describes the tip–sample interaction for the repulsive regime very well. This proves that the small amplitude FM-AFM image contrast obtained in the repulsive mode behaves like elastic contact mode imaging. Fitting a linear force law to the measured data leads to a contact stiffness of $\approx 58 \pm 1$ N m^{-1}. Nevertheless, in the repulsive mode the contrast formation tends to be more complicated. Here the tip is oscillating with a certain amplitude at close approach with respect to the sample surface. The grey shaded areas in figure 5 mark the force range at which the tip is oscillating over the sample surface in the attractive (figure 5(a)) and the repulsive (figure 5(b)) imaging regimes, respectively. For small oscillation amplitudes and the given set-point in the repulsive regime, the tip–sample distance stays always in the repulsive, contact-like, regime. Here, the tip–sample interaction is dominated by the repulsion between the surface and the tip ions. Due to a more complex inward displacement, a lateral in-plane distortion of the surface ions should be considered, when the repulsive force between the tip and the surface is originated. At such a close approach the situation becomes even more complicated due to substantial deformation of atoms both at the tip apex and the surface underneath. Elastic tip and sample deformations with a stick–slip type movement are likely to contribute to the imaging contrast. When the tip is dragged over the periodic potential defined by the atomic structure of the sample surface and the contact geometry, the tip tends to stick at a certain surface position until the force exerted by the moving support is high enough to slip to the next atomic position. The elastic energy stored in the system dissipates into tip and surface atoms by multiple phonon generation [36]. This atomic scale friction is often explained by the Tomlinson mechanism [21]. The shape of the force–distance curve in the repulsive regime implies that the tip strongly interacts with the sample surface. However, there is no indication of an adhesive neck formation between the tip and the substrate, which would be seen as a sharp increase in the attractive force due to surface tension. The absence of steps due to plastic deformations in the repulsive regime and hysteresis effects between forward and backward traces of the force–distance curve prove that the formation of an adhesive neck can be excluded.

A universal behaviour is predicted for the binding energy against distance curves of metallic systems [37]. In *ab initio* calculations, a simple two-parameter scaling is used to describe the adhesion and cohesion of metals, as well as the chemisorption of gas atoms on metal surfaces. Here we have started to analyse the binding energy–distance relation for a thin ionic film by recovering energy curves from measured frequency shift versus z-displacement. Integration of equation (1) gives the corresponding expression for the interaction energy $E(D)$ between the tip and the sample:

$$E(D) = \frac{2k}{f_0}\int_D^\infty \Delta f(z)\left((z-D) + \frac{A^{1/2}}{4}\sqrt{\frac{z-D}{\pi}} + \frac{A^{2/3}}{\sqrt{2(D-z)}}\right) \mathrm{d}z. \tag{4}$$

The recovered energy curve versus z-displacement shown in figure 6(a) can be scaled by

$$E^* = E/\Delta E \tag{5}$$

and

$$z^* = (z - z_m)/l \tag{6}$$

with ΔE being the maximum adhesion energy, z the interatomic separation distance, z_m the distance of separation at ΔE, and l a distance scaling parameter [38]. It was found that such a scaling of adhesion energy curves reduces them to a universal curve shape which is well described by the Rydberg function [39, 38]:

$$E^*(z^*) = -(1 + z^*)^{(-z^*)}. \tag{7}$$

In figure 6(b) the resulting relationship between scaled energy and distance is plotted, which is very well fitted by the Rydberg function with $\Delta E = 4.2$ aJ (26 eV) and $l = 0.3$ nm. The scaled energy versus distance curve falls on top of the universal Rydberg function described by equation (7). This suggests that while the magnitudes of adhesive energy and force are sensitive to tip geometry, material, and sample site being probed, the variation of the energy, or of the force, with tip–sample separation has a universal form independent of these variables, including tip shape. The good agreement

of the scaled curves in figure 6 also implies that the tip–sample contact is free of wetting effects and large plastic deformations. The determined scaling length, also referred to as decay length, is well in range with other experimentally determined values; for example, Schirmeisen *et al* reported a decay length of about 0.2 nm and maximum adhesive energy of $\Delta E = 3.4$ aJ (21 eV) for an atomically defined W(111) tip interacting with a Au(111) sample [40, 41]. Loppacher *et al* have measured a decay length of $l = 0.3$ nm for short-range metallic forces on Cu(111) and Cu(100) [42]. However, the experimentally determined decay lengths are significantly larger than the values predicted by theoretical models [39]. The relatively high decay length of 0.3 nm and an adhesive energy of $\Delta E = 4.2$ aJ (26 eV) cannot be explained by the interaction of one single apex atom of the tip with the sample surface. Therefore, it is likely that the determined values are caused by contributions from several tip and sample surface atoms. Substantial deformation of many atoms both at the tip apex and the surface underneath as well as the influence of the substrate has to be taken into account.

In conclusion, atomically resolved images on MgO(001) acquired in the attractive and the repulsive regimes reveal contrast changes. The importance of the tip-induced relaxation of the surface ions in the tip–surface interaction and in image contrast has been analysed. For the detailed interpretation of tip–sample interactions, distance-dependent frequency shift measurements have been performed. From the experimental data, the interaction force and energy between the tip and the sample have been recovered. The derived curves have been compared with specific force laws. The results demonstrate that elastic forces contribute significantly to the tip–sample interaction, even before the minimum of the force–distance curve is reached. A close relation between elastic deformations could be established at a distance where atomic resolution has been obtained in the attractive regime. The image contrast in the repulsive regime has been identified to be obtained in a contact-like mode, where a stick–slip-type motion seems to contribute significantly. The determined decay length and adhesion energy of the universal Rydberg fit emphasize the contribution of more than just one tip and sample surface atom.

Acknowledgments

It is a pleasure for MH to acknowledge useful discussions with U D Schwarz (Yale University, USA) and H Hölscher (University Münster, Germany). Also many thanks to J E Sader (University of Melbourne, Australia) for providing the Mathematica® code for implementing formulae (1) and (4). Financial support by the Austrian Science Fund (FWF) is gratefully acknowledged (MS).

References

[1] Giessibl F J 1995 Atomic resolution of the silicon(111)-(7 × 7) surface by atomic force microscopy *Science* **267** 68
[2] Kitamura K S and Iwatsuki M 1995 Observation of 7 × 7 reconstructed structure on the silicon (111) surface using ultrahigh-vacuum noncontact atomic-force microscopy *Japan. J. Appl. Phys.* **34** L145
[3] Allers W, Schwarz A, Schwarz U D and Wiesendanger R 1998 Scanning force microscope with atomic resolution in ultrahigh vacuum and at low temperatures *Rev. Sci. Instrum.* **69** 221
[4] Bammerlin M, Lüthi R, Meyer E, Baratoff A, Lü J, Guggisberg M, Loppacher C, Gerber C and Güntherodt H-J 1998 Dynamic SFM with true atomic resolution on alkali halide surfaces *Appl. Phys.* A **66** S293
[5] Tersoff J and Hamann D R 1983 Theory and application for the scanning tunneling microscope *Phys. Rev. Lett.* **50** 1998
[6] Shluger A L, Livshits A I, Foster A S and Catlow C R A 1999 Models of image contrast in scanning force microscopy on insulators *J. Phys.: Condens. Matter* **11** R295
[7] Hofer W A, Foster A S and Shluger A L 2003 Theories of scanning probe microscopes at the atomic scale *Rev. Mod. Phys.* **75** 1287
[8] Schwarz A, Allers W, Schwarz U D and Wiesendanger R 2000 Dynamic-mode scanning force microscopy study of n-InAs(110)-(1 × 1) at low temperatures *Phys. Rev.* B **61** 2837
[9] Weiss P S and Eigler D M 1993 What is underneath? Moving atoms and molecules to find out *Nanosources and Manipulations of Atoms under High Fields and Temperatures: Applications* (*NATO ASI Series E* vol 235) ed V T Binh, N Garcia and K Dransfeld (New York: Plenum)
[10] Cleveland J P, Manne S, Bocek D and Hansma P K 1993 A nondestructive method for determining the spring constant of cantilevers for scanning force microscopy *Rev. Sci. Instrum.* **64** 403–5
[11] Matthees W 2005 private communication
[12] Albrecht T R, Grütter P, Horne D and Rugar D 1991 Frequency modulation detection using high-Q cantilevers for enhanced force microscope sensitivity *J. Appl. Phys.* **69** 668
[13] Heyde M, Kulawik M, Rust H-P and Freund H-J 2004 Double quartz tuning fork sensor for low temperature atomic force and scanning tunneling microscopy *Rev. Sci. Instrum.* **75** 2446
[14] Heyde M, Sterrer M, Rust H-P and Freund H-J 2005 Atomic resolution on MgO(001) by atomic force microscopy using a double quartz tuning fork sensor at low-temperature and ultrahigh vacuum *Appl. Phys. Lett.* **87** 083104
[15] Bennewitz R, Foster A S, Kantorovich L N, Bammerlin M, Loppacher C, Schar S, Guggisberg M, Meyer E and Shluger A L 2000 Atomically resolved edges and kinks of NaCl islands on Cu(111): experiment and theory *Phys. Rev.* B **62** 2074
[16] Bennewitz R, Schar S, Gnecco E, Pfeiffer O, Bammerlin M and Meyer E 2004 Atomic structure of alkali halide surfaces *Appl. Phys.* A **78** 837
[17] Barth C and Henry C R 2003 Atomic resolution imaging of the (001) surface of UHV cleaved MgO by dynamic scanning force microscopy *Phys. Rev. Lett.* **91** 196102
[18] Kantorovich L N, Shluger A L and Stoneham A M 2001 Recognition of surface species in atomic force microscopy: optical properties of a Cr^{3+} defect at the MgO(001) surface *Phys. Rev.* B **63** 184111
[19] Giessibl F J and Reichling M 2005 Investigating atomic details of the CaF_2(111) surface with a qplus sensor *Nanotechnology* **16** S118
[20] Gnecco E, Bennewitz R, Gyalog T and Meyer E 2001 Friction experiments on the nanometre scale *J. Phys.: Condens. Matter* **13** R619
[21] Tomlinson G A 1929 A molecular theory of friction *Phil. Mag.* **7** 905
[22] Hölscher H, Schwarz U D and Wiesendanger R 1996 Simulation of a scanned tip on a NaF(001) surface in friction force microscopy *Europhys. Lett.* **36** 19
[23] Hölscher H, Schwarz U D, Zwörner O and Wiesendanger R 1998 Consequences of the stick–slip movement for the scanning force microscopy imaging of graphite *Phys. Rev.* B **57** 2477
[24] Sader J E and Jarvis S P 2004 Accurate formulas for interaction force and energy in frequency modulation force spectroscopy *Appl. Phys. Lett.* **84** 1801

[25] Giessibl F J 1997 Forces and frequency shifts in atomic-resolution dynamic-force microscopy *Phys. Rev.* B **56** 16010
[26] Israelachvili J N 1992 *Intermolecular and Surface Forces* 2nd edn (London: Academic Press)
[27] Stillinger F H and Weber T A 1985 Computer simulation of local order in condensed phases of silicon *Phys. Rev.* B **31** 5262
[28] Livshits A I, Shluger A L, Rohl A L and Foster A S 1999 Model of noncontact scanning force microscopy on ionic surfaces *Phys. Rev.* B **59** 2436
[29] Hallmark V M, Chiang S, Rabolt J F, Swalen J D and Wilson R J 1987 Observation of atomic corrugation on Au(111) by scanning tunneling microscopy *Phys. Rev. Lett.* **59** 2879
[30] Wintterlin J, Wiechers J, Brune H and Gritsch T 1989 Atomic-resolution imaging of close-packed metal-surfaces by scanning tunneling microscopy *Phys. Rev. Lett.* **62** 59
[31] Sugawara Y, Ohta M, Ueyama H, Morita S, Osaka F, Ohkouchi S, Suzuki M and Mishima S 1996 Atomic resolution imaging of InP(110) surface observed with ultrahigh vacuum atomic force microscope in noncontact mode *J. Vac. Sci. Technol.* B **14** 953
[32] Hertz H 1882 Über die berührung fester elastischer Körper *J. Reine Angew. Math.* **92** 156
[33] Schwarz U D, Zwörner O, Köster P and Wiesendanger R 1997 Quantitative analysis of the frictional properties of solid materials at low loads. I. Carbon compounds *Phys. Rev.* B **56** 6987
[34] Enachescu M, van den Oetelaar R J A, Carpick R W, Ogletree D F, Flipse C F J and Salmeron M 1998 Atomic force microscopy study of an ideally hard contact: the diamond(111)/tungsten carbide interface *Phys. Rev. Lett.* **81** 1877
[35] Hölscher H, Schwarz A, Allers W, Schwarz U D and Wiesendanger R 2000 Quantitative analysis of dynamic-force-spectroscopy data on graphite(0001) in the contact and noncontact regimes *Phys. Rev.* B **61** 12678
[36] Buldum A, Leitner D M and Ciraci S 1999 Model for phononic energy dissipation in friction *Phys. Rev.* B **59** 16042
[37] Rose J H, Ferrante J and Smith J R 1981 Universal binding-energy curves for metals and bimetallic interfaces *Phys. Rev. Lett.* **47** 675
[38] Banerjea A, Smith J R and Ferrante J 1990 Universal aspects of adhesion and atomic force microscopy *J. Phys.: Condens. Matter* **2** 8841
[39] Rose J H, Smith J R and Ferrante J 1983 Universal features of bonding in metals *Phys. Rev.* B **28** 1835
[40] Schirmeisen A, Cross G, Stalder A, Grütter P and Dürig U 2000 Metallic adhesion forces and tunneling between atomically defined tip and sample *Appl. Surf. Sci.* **157** 274
[41] Schirmeisen A, Cross G, Stadler A, Grütter P and Dürig U 2000 Metallic adhesion and tunneling at the atomic scale *New J. Phys.* **2** 29
[42] Loppacher Ch, Bammerlin M, Guggisberg M, Schär S, Bennewitz R, Baratoff A, Meyer E and Güntherodt H-J 2000 Dynamic force microscopy of copper surfaces: atomic resolution and distance dependence of tip–sample interaction and tunneling current *Phys. Rev.* B **62** 16944